Measurement and modelling of the transient thermal-mechanical strain field during GMA welding

H. E. Coules[1], L. D. Cozzolino[1], P. Colegrove[1], S. W. Wen[2]

[1] Cranfield University, Cranfield, Bedfordshire, MK43 0AL, United Kingdom

[2] Tata Steel R, D & T, Swinden Technology Centre, Rotherham, South Yorkshire, S60 3AR, United Kingdom

The state of residual stress in welded joints is a well-studied topic, and many methods of residual stress measurement are now available. However, far less is known about the transient strains which occur during the welding process, even though these are the direct cause of residual stresses. Efforts to model welding processes usually include transient stresses and strains among their results, but in general these models can only be easily compared against experimentally measured residual stresses: there is a lack of published data covering strain in the transient regime.

In this study, electrical resistance strain gauges were used to measure transient strains during welding, and comparison is made between these measurements and the results from a sequential thermo-mechanical finite element model of the process. Well-defined mechanical boundary conditions were used for the experiments to ease interpretation of the measured strain data, and to enable close approximation with the boundary conditions of the computational model. The transient biaxial state of strain was measured during Gas Metal Arc Welding (GMAW) of S355 steel samples in a bead-on-plate configuration. Measured transient strains were found to be consistent between samples, and showed good agreement with the modelling results. It is hoped that future study of welding transient strains will aid in the optimisation of in-process methods to reduce residual stress, such as rolling and quench cooling.

1   Introduction

During welding, significant residual stresses are produced by differential thermal expansion of material under a non-uniform thermal field. As it cools, material close to the source of heat input is constrained by material further away, generally resulting in high tensile residual stresses in an area around the weld seam. These tensile stresses can have a negative impact on the mechanical properties of the joint, aiding both

1

fatigue cracking [1] and brittle fracture [2]. They also cause distortion of the component, a problem which is especially evident in the welding of thin materials, which are prone to buckling.

Several methods for reducing residual stress, including local rolling [3], global mechanical tensioning [4], and the use of trailing impingement cooling [5] have been used during the welding process to inhibit the initial formation of residual stresses. To enable the best use of such *in situ* techniques, it will be necessary to characterise the transient thermal stress and strain fields present in the parent material while welding takes place. This will allow the design of processes which can more precisely counteract the thermal stress field.

While many computational models have been developed to study the mechanical effects of welding, verification of mechanical modelling is most often done by comparison of residual stresses only. As is evident from a summary of experimentally verified models by Lindgren [6], the transient strains are seldom compared. Early experiments on measuring welding thermal strains were carried out under the supervision of Masubuchi [7, 8, 9]. Although the results were mixed, they did prove the concept of using resistance strain gauges to measure welding strains *in situ*. More recently, optical Fibre Bragg Grating (FBG) sensors have also been shown to be suitable for such *in situ* measurements [10, 11]

2   Experimental

2.1   Sample description

Five bead-on-plate welds were carried out using the sample layout shown in Figure 1. The material used for the experimental samples was 3 mm S355 mild steel supplied in the as-rolled condition. The welds were carried out in a single pass using pulsed GMAW; the welding parameters were designed to achieve full penetration of the weld pool through the plate thickness, and are given in Table 1.

2
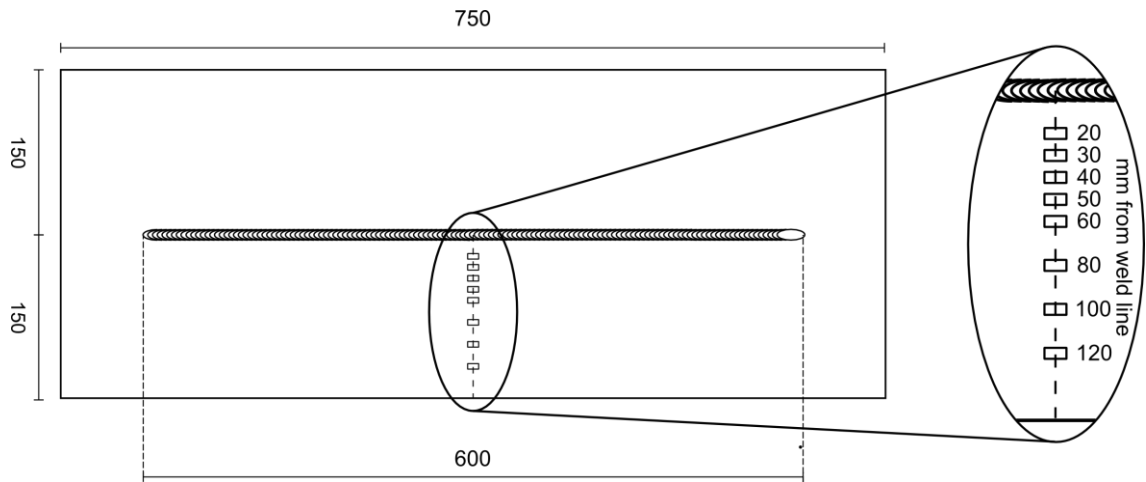
Figure 1: Sample layout for strain gauge tests (dimensions in mm).

Table 1: Welding parameters.

Process	GMAW (pulsed)
Power supply	Fronius TransPuls Synergic 5000
Contact tip to work distance	13 mm
Torch angle	90°
Filler wire diameter	1 mm
Filler wire feed speed	173 mm s^{-1}
Travel speed	10.8 mm s^{-1}
Current	270 A
Voltage	27.8 V
Gas composition	20% CO_2, 2% O_2, balance Ar
Gas flow rate	200 ml s^{-1}

2.2   Sample restraint

During testing, the samples were held flat using a vacuum clamping system, which applied a vacuum to the underside of the plates. This method was chosen since it allowed complete access to the top side of the samples for strain gauge and thermocouple attachment. It is also very simple to model compared with other types of clamping: a steady, even pressure is applied over almost the entire plate area, and there are no local stress concentrators. Finally, the system holds all parts of the plate completely flat during the experiment, meaning that only strains due to in-plane deformation are measured by the strain gauges. No out-of-plane bending of the sample

3

occurs until it is unclamped, which greatly simplifies interpretation of the strain gauge data.

2.3   Strain and temperature measurements

The strain measurements were carried out using foil resistance strain gauges attached to the upper side of the sample, in a line running from the weld seam to the edge of the plate as shown in Figure 1. Elevated-temperature gauges (Micro-Measurements WK-series) were used at the 20 and 30 mm positions, while standard types (CEA and L2A-series) were used elsewhere. Three of the five samples had uniaxial gauges attached at all eight locations. The fourth had the gauges at 20 and 30 mm substituted for three-gauge rectangular rosettes, while the final sample employed rosettes at 40, 50, 60 and 80 mm, and uniaxial gauges elsewhere. Rosettes could not be employed at all locations simultaneously due to the limited number of channels available on the data logging equipment.

The strain at a point on the sample consists of a plastic component ε_p, a thermal component ε_t due to thermal dilation of the material at that point, and an elastic component ε_e due to the stress state. Hence the total strain ε is given by:

$$\varepsilon = \varepsilon_t + \varepsilon_e + \varepsilon_p \qquad \text{(Eqn. 1)}$$

In these experiments, all the strain gauges were self-temperature-compensating, and had the same coefficient of thermal expansion as the base material. This ensured that only the plastic and elastic components of strain were measured. The strain readings were also compensated for temperature effects on the transducer itself, as per the manufacturer's recommendations [12]. Wherever strain rosettes were employed, the usual strain transformation equations were used to calculate strain components in the coordinates of the plate [ε_{xx}, ε_{yy}, γ_{xy}] from the rosette strains and gauge orientation [13]. It was then possible to calculate stresses in the longitudinal and transverse directions using Hooke's law for plane stress:

$$\begin{bmatrix} \sigma_{xx} \\ \sigma_{yy} \\ \tau_{xy} \end{bmatrix} = \begin{bmatrix} \dfrac{E}{1-v^2} & \dfrac{vE}{1-v^2} & 0 \\ \dfrac{vE}{1-v^2} & \dfrac{E}{1-v^2} & 0 \\ 0 & 0 & \dfrac{E}{2(1+v)} \end{bmatrix} \begin{bmatrix} \varepsilon_{xx} \\ \varepsilon_{yy} \\ 2\varepsilon_{xy} \end{bmatrix} \qquad \text{(Eqn. 2)}$$

where E and v are the Young's modulus (210 GPa) and the Poisson ratio (0.3) respectively. It should be noted that this method assumes the material to be linearly elastic (see Section 4.2).

4

Thermocouples were used to determine the temperature at the gauge locations 20, 30, 40, and 50 mm from the weld line. Preliminary experiments showed that the temperature change at 60, 80, 100 and 120 mm was too small to affect the strain measurement. Aluminium tape and glass fibre insulation was used to protect the measurement area from arc radiation, and the addition of this protective layer was shown not to affect the temperature field in the sample significantly.

An external sensor was used to determine the instant when the arc passed the line of strain gauges, which simplified the comparison of data collected from separate samples. All measurements were logged to a PC at a frequency of 2 Hz using a National Instruments CompactDAQ modular data acquisition unit.

3   Modelling

3.1   Overview

A three-dimensional finite element model of the welding process was developed using Abaqus software. A sequential thermal-mechanical analysis was performed using a single mesh comprising 56,475 elements. Quadratic brick-type elements were used for the thermal part of the analysis, while the mechanical analysis used linear brick elements with the same mesh.

The model had the same dimensions as the experimental sample, however due to symmetry about the weld line only one half of the object was modelled. Deposition of the raised weld bead resulting from the GMAW process was not simulated; the weld bead material was assumed to exist from the start of the weld. Further details of the modeling techniques used are given elsewhere [14].

3.2   Heat source

To simulate the heat input from the welding arc, the model used a double-ellipsoid heat source of the type developed by Goldak et al. [15]. The heat source dimensions were based on empirical measurements of the size of the weld pool, while the total heat input was based the actual welding parameters. An arc thermal efficiency of 77% was assumed, a typical value for the GMAW process [16, 17].

3.3   Boundary conditions

Thermal conduction from the sample to the backing bar and clamping bed was modelled using simple convective heat transfer. The heat transfer coefficients used in the model were tuned so as to approximate a temperature field similar to that measured experimentally (see Figure 2). In the case of conduction into the backing bar,

5

the heat transfer coefficients were defined as an exponential function of temperature, however constant coefficients were used elsewhere. The mechanical restraint provided by the vacuum clamping system was modelled by preventing displacement of the lower surface of the model in the vertical (z) direction. Along the weld line, displacement in the transverse (y) direction and rotation in the y-z and x-y planes was prevented, to simulate the condition of symmetry at this side of the model.
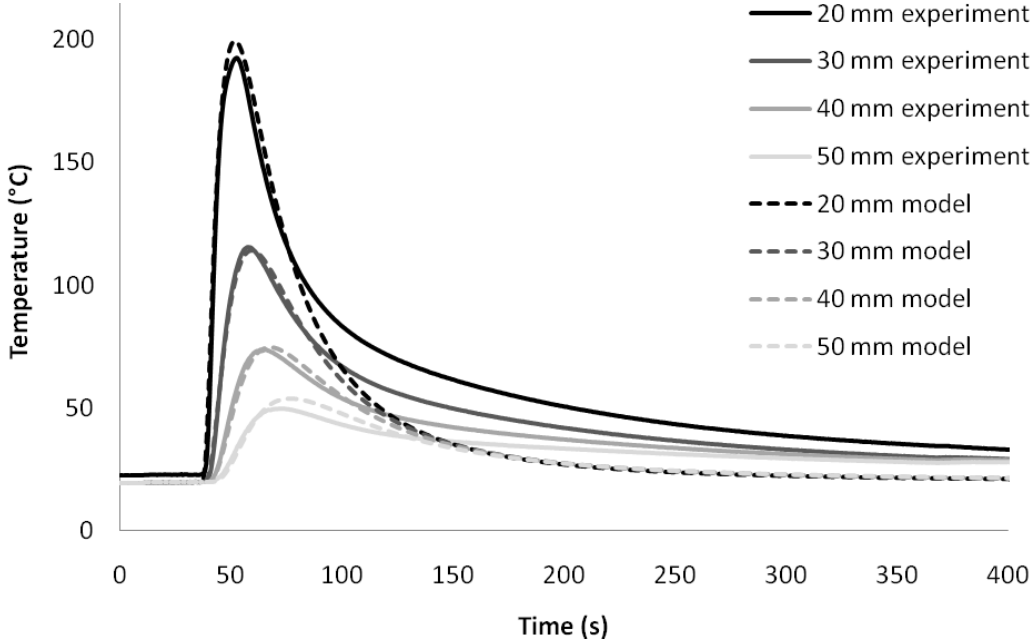

Figure 2: Comparison between modelled and experimental temperature distributions.

4   Results and discussion

4.1   Repeatability of strain measurements

Figure 3 shows a plot of strain in the longitudinal direction, 30 mm from the weld line, for the five welds made. Welding takes place between -28s and +28s, with the arc passing the measurement line (see Figure 1) at 0s. After completion of welding, the plate is allowed to cool (+28s onwards). Close agreement between samples can be seen for the initial transient region during the weld, although there is some divergence during cooling, resulting in a range of residual strains. It is suggested that this discrepancy is caused by small sample-to-sample variations in heat transfer, clamping conditions, initial residual stresses, or a combination of these factors.

6
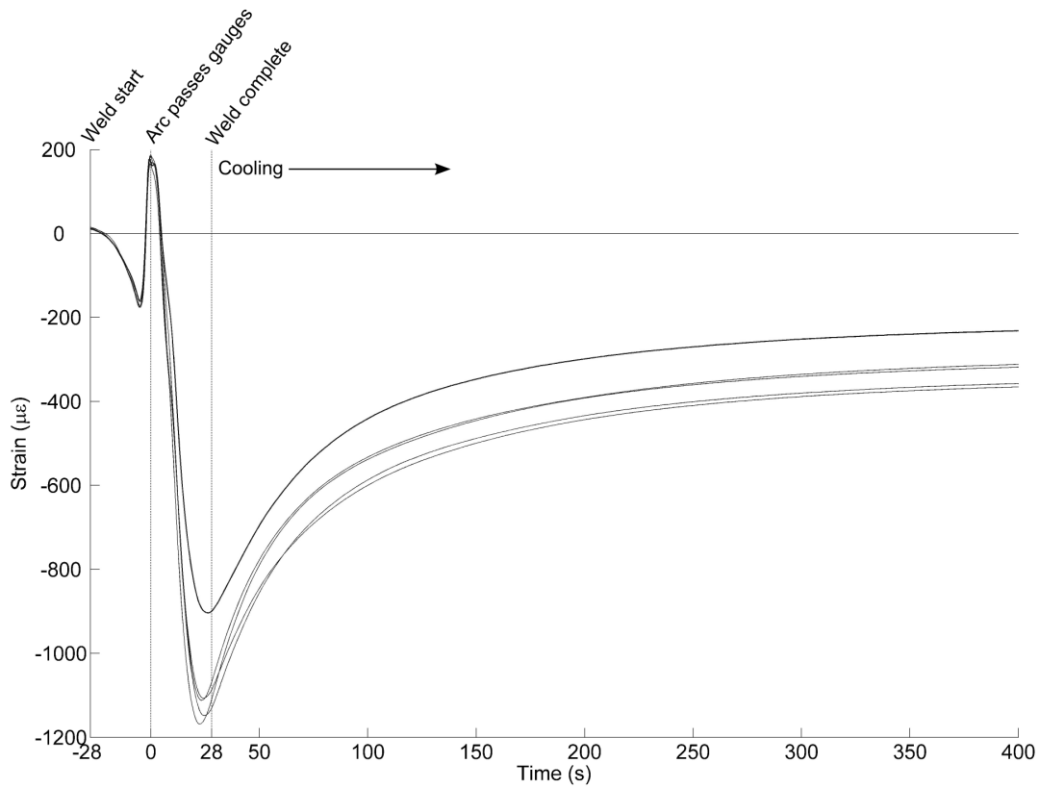
Figure 3: Strain in the longitudinal direction, 30 mm from the weld line, for five identical bead-on-plate samples.

4.2 Calculation of biaxial state of stress

For the calculation of the transient stress from the strain data using Hooke's law (see Section 2.3), the material is assumed to be both isotropic and linearly elastic. Therefore, the stress can only be calculated via this method if the material undergoes purely elastic deformation during the measurement. Fortunately, no plastic yield was observed at any of the gauge locations (see Figure 4c), although the peak compressive strains measured by some of the gauges closest to the weld line did reach 80-90% of the yield strain of the material. From the absence of yielding at any of the gauge locations it can be inferred that in this case, all of the thermally-induced plastic deformation caused by the welding process occurs within 20 mm of the weld line.

The calculation of stresses using Hooke's law also makes the assumption that the plate is initially unstressed at the start of welding, so that any strain increment from this point corresponds to the total stress in the plate. Although residual stresses are known to exist in rolled material of this type, it is likely that they are small in comparison to the large stresses induced by welding.

7

By calculating the stresses at a number of strain rosette locations and plotting them over time, it is possible to produce a map of stress for the region where rosette measurements were taken. Data from two identical specimens with rosettes in different locations (see Section 2.3) were used in this way to produce the plots in Figure 4. As in most linear welds, the largest stresses observed are in the longitudinal direction: Figure 4a shows the longitudinal component of stress between 20 and 80 mm from the weld centreline as the arc passes by. Initially unstressed at -20s, the material experiences a small compressive 'bow wave' at around -4s as the heat source approaches. As the arc passes, it heats the material close to the weld line, which expands, causing compression in the weld region and a balancing tensile stress in the far field (0 to +20s). However, the heat rapidly conducts outwards and the central material cools and contracts, causing tensile stresses directly along the weld line, while compressive stresses develop further away from it (+20 to +60s and beyond). Overall, the transient distribution of stress is similar to that predicted by most previous models of linear welds [4, 18, 19, 20, 21].

8
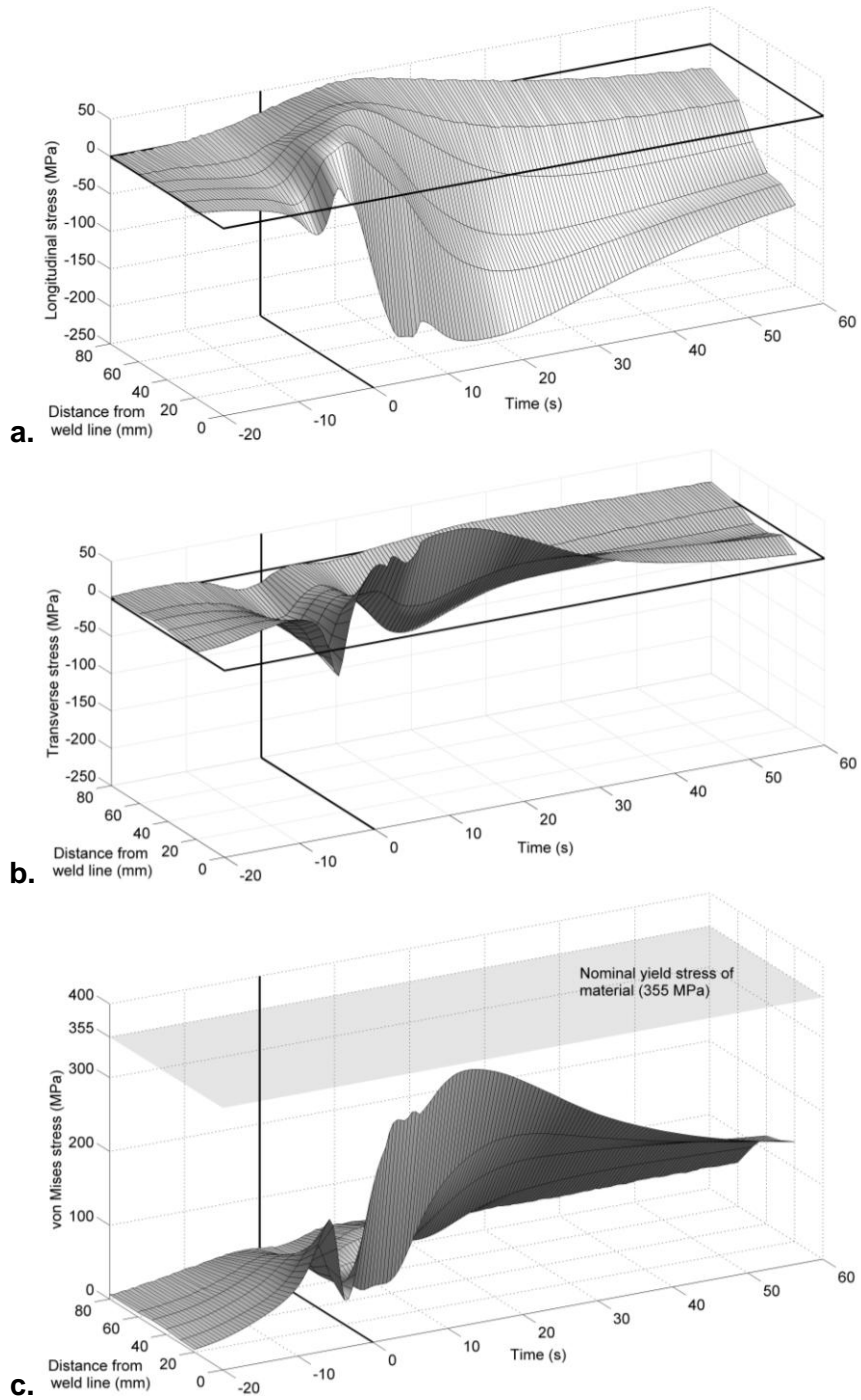
Figure 4: Measured stress components in a plate sample during GMAW: a. longitudinal, b. transverse, and c. von Mises. The arc passes the measurement line at 0s.

4.3   Comparison of model with experiment

Figure 5 shows a comparison of measured and modelled transient stresses. Qualitatively, the results are very similar: the development of stress over the transient region agrees well, however there are some differences in the magnitudes of the transient stresses. The most obvious difference between the measured and modelled cases is the disparity between the peak compressive stresses at 20 mm from the weld centerline, and the small inflection in measured stress at this point approximately 8 seconds after the arc pass. This inflection (and the subsequently reduced peak compared with the model) was a consistent feature of all the measurements taken at this distance, and is thought to be caused by effects of the $\gamma \rightarrow \alpha$ phase transformation at the weld line, which were not included in the model.
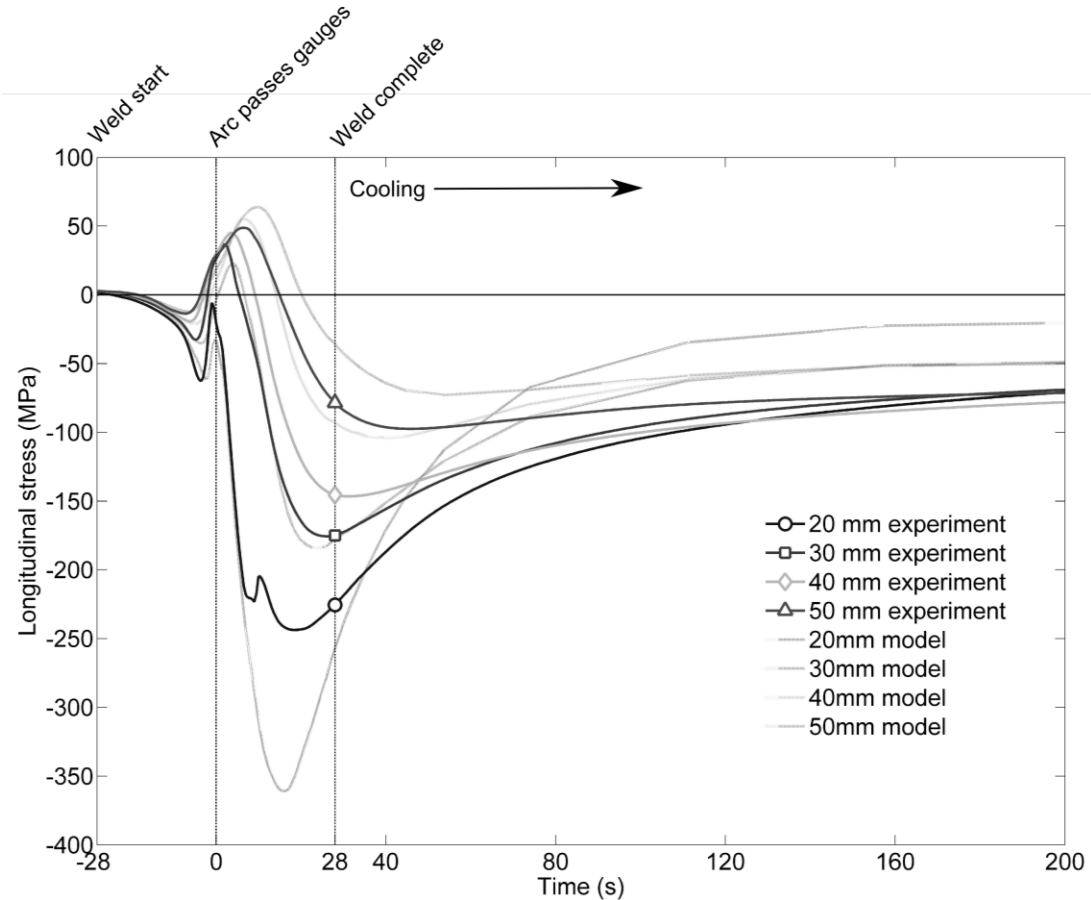

Figure 5: Comparison of modelled and measured longitudinal stress at different distances from the weld line.

4.4 Estimation of residual stresses

The stress calculated from strain rosette readings after cooling of the sample is an indication of the residual stress introduced by welding. As shown in Figure 6, the modelled residual stresses compare well with stresses calculated by this method. Unfortunately, the high temperature during welding limits the proximity of the strain gauges to the weld line, so the central tensile peak in residual stress cannot be directly measured from the strain data. However, since the residual stresses must be self-equilibrating over a section of the sample, the magnitude of the compressive residual stresses is an indicator of the level of tensile stress in the weld region.

This method of estimating residual stresses using strain gauges attached throughout the welding process is simple to apply and entirely non-destructive. In theory, these kinds of measurements could be used to rapidly assess the effectiveness of residual stress mitigation methods.
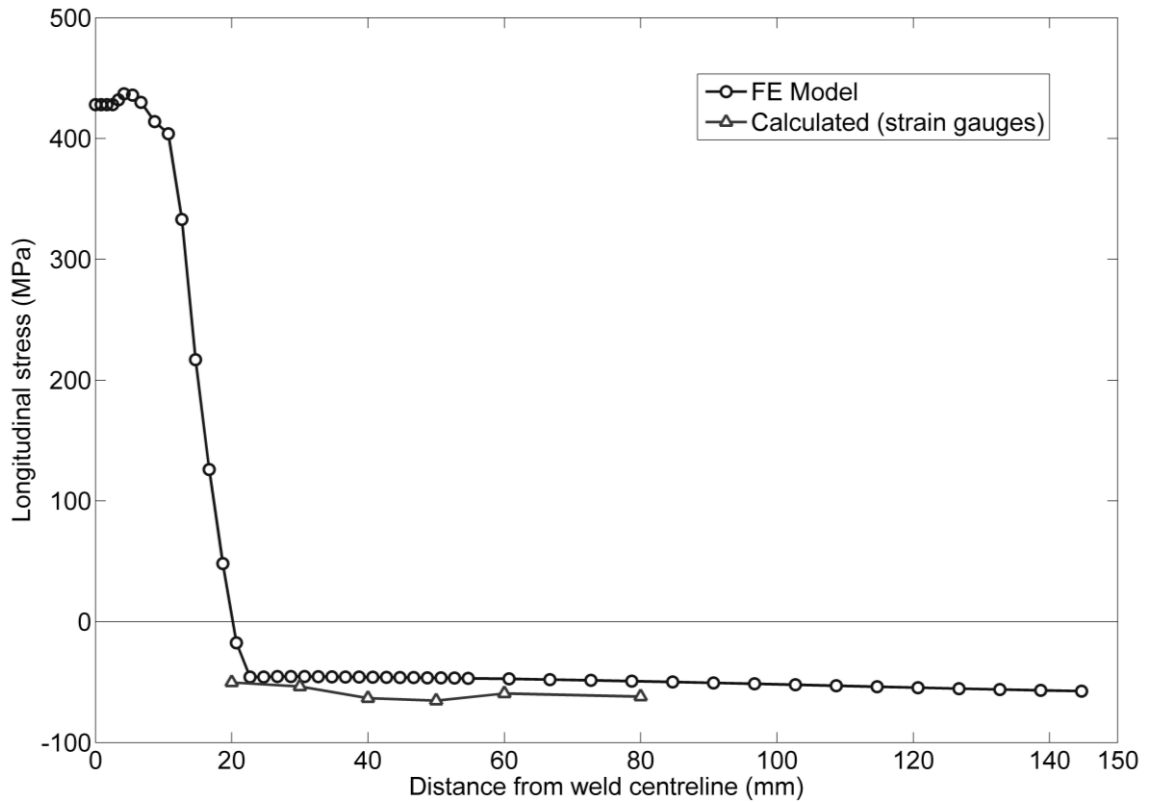
Figure 6: Longitudinal residual stress across the plate section (prior to unclamping).

5   Conclusions

In this paper, we have demonstrated the following:

- Measurement of transient strains during GMA welding of steel plate specimens using foil resistance strain gauges. The repeatability of this method has also been shown.

- Calculation *via* Hooke's law of the transient biaxial state of thermally-induced stress due to welding from measured strain data. By plotting the stress variation over time at several locations, the stress state around the advancing welding torch can be visualized (Figure 4). However, the assumption of a linear elastic material in this method prevents the calculation of stress for regions very close to the weld line.

- Transient stresses calculated from the experimental data compare well with the results of a finite element model of the process which was developed for this investigation, and are in qualitative agreement with previously reported modelling results from other sources.

- Residual stresses away from the weld line can be estimated, nondestructively, using the final strains measured at the end of the welding process. This method of residual stress estimation is conceptually simple and easy to apply in practice. However, values of residual stress calculated this way may be affected by pre-existing stresses within the material.

6   Acknowledgements

7   References

[1]   S. J. Maddox. *Fatigue strength of welded structures.* Abington Publishing, Cambridge, UK, 2nd edition, 1991.

[2]   R. A. Ainsworth, J. K. Sharples, and S. D. Smith. Effects of residual stresses on fracture behaviour - experimental results and assessment methods. *Journal of Strain Analysis for Engineering Design*, 35(4):307–316, 2000.

[3]   J. Altenkirch, A. Steuwer, P. Withers, S. Williams, M. Poad, and S. W. Wen. Residual stress engineering in friction stir welds by roller tensioning. *Science and Technology of Welding and Joining*, 14(2):185–192, 2009.

[4]   D. G. Richards, P. B. Prangnell, S. W. Williams, and P. J. Withers. Global mechanical tensioning for the management of residual stresses in welds. *Materials Science and Engineering A*, 489(1-2):351–362, 2008.

[5]   E. M. van der Aa. *Local cooling during welding: prediction and control of residual stresses and distortion*. PhD thesis, Delft University of Technology, 2007.

[6]   L.-E. Lindgren. Finite element modeling and simulation of welding. part 3: Efficiency and integration. *Journal of Thermal Stresses*, 24(4):305–334, 2001.

[7]   K. M. Klein and K. Masubuchi. Investigation of welding thermal strains in high-strength steels for marine application. In *2nd International Ocean Development Conference, Tokyo, Japan*, 1972.

[8]   F. M. Pattee. Buckling distortion of thin aluminium plates during welding. Master's thesis, Massachusetts Institute of Technology, 1975.

[9]   J.-S. Hwang. Residual stresses in weldments in high-strength steels. Master's thesis, Massachusetts Institute of Technology, 1976.

[10]   J. C. Suárez, B. Remartinez, J. M. Menéndez, A. Güemes, and F. Molleda. Optical fibre sensors for monitoring of welding residual stresses. *Journal of Materials Processing Technology*, 143-144(1):316–320, 2003.

[11]   V. Richter-Trummer, S. O. Silva, D. F. C. Peixoto, O. Frazao, P. M. G. P. Moreira, J. L. Santos, and P. M. S. T. De Castro. Fibre bragg grating sensors for monitoring the metal inert gas and friction stir welding processes. *Measurement Science and Technology*, 21(8), 2010.

[12]   Vishay. Strain gage thermal output and gage factor variation with temperature. Technical Report TN-504-1, Vishay Precision Group, 2010.

[13]   C. C. Perry and H. R. Lissner. *The strain gage primer*. McGraw-Hill, New York, 1962.

[14]   L. D. Cozzolino, H. E. Coules, P. Colegrove, and S. W. Wen. Modelling distortion reduction on pre- and post-weld rolled gas metal arc welded plates. In *Proceedings of the IWOTE'11*, 2011. under review.

[15]   J. Goldak, A. Chakravarti, and M. Bibby. A new finite element model for welding heat sources. *Metallurgical Transactions B*, 15(2):299–305, 1984.

[16]   J. N. DuPont and A. R. Marder. Thermal efficiency of arc welding processes. *Welding Journal*, 74(12):406–s, 1995.

[17]   M. Lu and S. Kou. Power inputs in gas metal arc welding of aluminum - part 2. *Welding Journal*, 68:452s, 1989.

13

[18]   T. Inoue. *Processes and mechanisms of welding residual stress and distortion*, chapter 3: Thermal-metallurgical-mechanical interactions during welding, pages 99–125. Woodhead Publishing, 2005.

[19]   F. A. Soul and Y.-H. Zhang. Numerical study on stress induced cambering distortion and its mitigation in welded titanium alloy sheet. *Science and Technology of Welding and Joining*, 11(6):688–693, 2006.

[20]   P. Tekriwal and J. Mazumder. Transient and residual thermal strain-stress analysis of gmaw. *Journal of Engineering Materials and Technology, Transactions of the ASME*, 113(3):336–343, 1991.

[21]   N. S. Al-Huniti, M. A. Al-Nimr, and M. A. Da'as. Transient variations of thermal stresses and the resulting residual stresses within a thin plate during welding processes. *Journal of Thermal Stresses*, 27(8):671–689, 2004.